Composite Structures 93 (2011) 2663–2670

Contents lists available at ScienceDirect

Composite Structures

journal homepage: www.elsevier.com/locate/compstruct

Hybrid layerwise-differential quadrature transient dynamic analysis of functionally graded axisymmetric cylindrical shells subjected to dynamic pressure

A.R. Setoodeh [a,*], M. Tahani [b], E. Selahi [b,c]

[a] Faculty of Mechanical & Aerospace Engineering, Shiraz University of Technology, Shiraz, Iran
[b] Department of Mechanical Engineering, Faculty of Engineering, Ferdowsi University of Mashhad, Mashhad, Iran
[c] Marine Industry Organization, Shiraz, Iran

ARTICLE INFO

Article history:
Available online 5 July 2011

Keywords:
Transient dynamic analysis
Functionally graded materials
Cylindrical shells
Differential quadrature method
Layerwise theory
Newmark's time integration

ABSTRACT

In this paper, two computationally efficient and accurate solution methods for transient dynamic analysis of functionally graded (FG) cylindrical shells subjected to internal dynamic pressure are presented. In order to accurately account for the thickness effects, the layerwise theory is employed to approximate the displacement components in the radial direction. In the first solution method, differential quadrature method (DQM) is implemented to discretize the resulting equations in the both spatial and time domains. In the second approach, DQM is applied to discretize equations in the axial direction while Newmark's time integration scheme is used to solve the problem in the time domain. The fast convergence rate of the methods is demonstrated and their accuracy is verified by comparing the results with those obtained using ANSYS and also with available exact solution of a particular problem. Considerable less computational efforts of the proposed approaches with respect to the finite element method is observed. Furthermore, comparative studies are performed between two approaches in different cases and it is found that the two techniques give very close results. The effects of geometrical parameters and boundary conditions on the transient behavior of shells are also investigated.

1. Introduction

Functionally gradient structures are a new class of composites that have a continuous and smooth variation of material properties from one surface to the other. Despite the fact that anisotropic laminated composites often suffer from stress concentrations near material and geometric discontinuities, the gradation in material properties of FG structures reduces thermal and residual stresses [1]. Most of functionally graded materials (FGMs) are made of ceramic and metal. Ceramic material provides a high temperature resistance due to its low thermal conductivity, and metal constituent largely improves load-bearing capacity. Recently, FG shells are widely used in many engineering applications such as aerospace, marine and automobile structures which are mostly subjected to vibration and dynamic loadings. Hence, it is of a great importance to understand the dynamic behavior of FG shells for the design of aforementioned structures.

Over the past decade, research on FG shells focused mainly on static deformation and vibrational response of these structures. However, due to their evident key role in practical applications, the study on dynamic behavior of FG cylindrical shells has recently attracted the attention of many researchers [2]. Awaji and Sivakuman [3] studied thermo-mechanical behavior of a FG hollow circular cylinder subjected to mechanical loads and linearly increasing temperature. Sofiyev and Schnack [4] investigated the stability of cylindrical thin FG shells under torsional loading varied as a linear function of time. Wang et al. [5] investigated transient temperature and associated thermal stresses in FGMs using finite element/finite difference (FE/FD) methods. Zhu et al. [6] developed a three-dimensional (3D) theoretical model for analyzing the dynamic stability behavior of FG piezoelectric circular cylindrical shells subjected to a combined loading of periodic axial compression and electric field in the radial direction. Bahtui and Eslami [7] studied coupled thermoelastic response of a FG cylindrical shell under thermal shock load using higher-order shear deformation theory. Santos et al. [8], presented a semi-analytical finite element model for functionally graded cylindrical shells subjected to transient thermal shock loading, by using the three-dimensional linear elasticity theory.

Guo and Noda [9] studied the thermal stresses of a thin FG cylindrical shell due to a thermal shock. Peng and Li [10], considered transient response of temperature and thermal stresses in a FG hollow cylinder. Hosseini and Shahabian [11] and Shahabian and Hosseini [12], investigated reliability and safety evaluation of dynamic stresses for FG thick hollow cylinder subjected to sudden unloading due to mechanical shock loading.

* Corresponding author. Tel./fax: +98 711 7264102.
E-mail addresses: setoodeh@sutech.ac.ir, asetood@yahoo.com (A.R. Setoodeh).

0263-8223/$ - see front matter © 2011 Elsevier Ltd. All rights reserved.
doi:10.1016/j.compstruct.2011.06.011

Due to the complexity encounters in dynamic analysis of FG shells, exact solution is not available. Thus, a precised theory is needed to fully account the dynamic response compared to the 3D elasticity theory. It was also observed that when the shell structure becomes thicker, the tendency of thickness vibration becomes more important [13]. Displacement-based layerwise theories assume a separate displacement field within each subdivision. Therefore, layerwise theory improves the displacement field compared to equivalent single-layer theories. Besides, the computational cost is reduced with respect to 3D elasticity theory. For FGMs, Tahani and Mirzababaee [14] used a layerwise theory to analytically predict displacements and stresses in FG composite plates in cylindrical bending subjected to thermomechanical loadings.

Besides the precision, the computation cost is another critical parameter in modeling. Differential quadrature (DQ) is a numerical technique that is used since 1988. Bert and Malik [15,16] presented a review of the early developments in DQM. Malekzadeh and his co-workers [17–21] demonstrated that using DQM for solving the governing equations for different mechanical problems leads to highly accurate results with less computations.

To the best of authors' knowledge, there is no published paper on the analysis of FG shells by using the mixed layerwise DQM. In this paper, the transient dynamic behavior of FGM hollow cylindrical shells subjected to internal dynamic loading is investigated by DQM. The layerwise theory is used to improve the displacement field and, therefore, also strains and stresses with minimum computational cost. Both DQM and Newmark's time integration scheme are comparatively employed to solve the developed DQM discretized governing equations in the time domain. The accuracy, convergence and versatility of the algorithm are proved via different examples for both thin and thick shells. Also, the effects of geometrical parameters and different boundary conditions are demonstrated.

2. Mathematical modeling

Consider a FG hollow circular cylindrical shell with varying material properties in the thickness direction. The thickness, length, inner radius and outer radius of the shell are denoted by h, l, r_{in} and r_{out} respectively, as shown in Fig. 1. A cylindrical coordinate system (r, θ, z) is used to label the material point of the shell referring to the radial, circumferential and axial directions and u, v and w denote the corresponding displacement components.

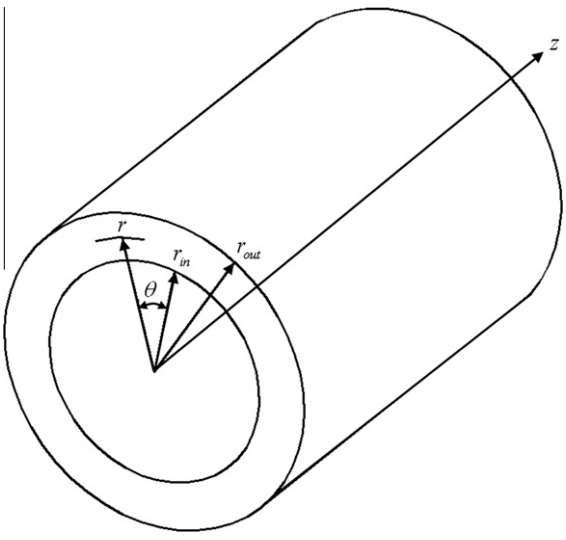

Fig. 1. Configuration of the FGM shell.

2.1. FGM properties modeling

In this modeling, the variations of the modulus of elasticity E and the mass density ρ through the thickness are assumed to be in terms of a power law distribution function as follows:

$$E(r) = E_m\left(\frac{r}{r_{in}}\right)^{n_1}, \quad \rho(r) = \rho_m\left(\frac{r}{r_{in}}\right)^{n_2} \tag{1}$$

A constant Poisson's ratio v is assumed. In these equations E_m and ρ_m are fully metallic modulus of elasticity and density in the inner surface r_{in}, and subscripts m and c refer to the metal and ceramic constituents which represent the materials the inner and outer surface of the shell are made of, respectively. Also n_1 and n_2 are the power law exponents.

2.2. Equations of motion in layerwise theory

The displacement field in the form of layerwise theory for axisymmetric cylindrical shells is as follows:

$$\begin{aligned} u(r,z,t) &= \sum_{i=1}^{N_r} U_i(z,t)\varphi_i(r) = U_i(z,t)\varphi_i(r) \\ w(r,z,t) &= \sum_{i=1}^{N_r} W_i(z,t)\varphi_i(r) = W_i(z,t)\varphi_i(r) \end{aligned} \tag{2}$$

where $U_i(z,t)$ and $W_i(z,t)$ denote the displacement components at the bottom of ith mathematical layer in the r and z-direction, respectively; $\varphi_i(r)$ is a continuous function in terms of the thickness coordinate r; also N_r represents the number of nodes in the r-direction of the shell, which depends on the number of considered mathematical layers N_e through the thickness.

The global linear interpolation function in the ith mathematical layer is defined as below:

$$\varphi_i(r) = \begin{cases} 0 & r \leqslant r_{i-1} \\ \frac{r-r_{i-1}}{h_{i-1}} & r_{i-1} \leqslant r \leqslant r_i \\ \frac{r_{i+1}-r}{h_i} & r_i \leqslant r \leqslant r_{i+1} \\ 0 & r \geqslant r_{i+1} \end{cases}, \quad i = 1,2,\ldots,N_r \tag{3}$$

where h_i is the thickness of the ith layer and r_i denotes the radial coordinate of the ith surface. Fig. 2 presents the through-thickness approximation of the displacement field. The strain–displacement relations for axisymmetric cylindrical shells based on the layerwise theory become:

$$\begin{aligned} \varepsilon_r(r,z,t) &= U_i(z,t)\frac{d\varphi_i(r)}{dr}, \quad \varepsilon_\theta(r,z,t) \\ &= \frac{U_i(z,t)\varphi_i(r)}{r}, \quad \varepsilon_z(r,z,t) \\ &= \frac{\partial W_i(z,t)}{\partial z}\varphi_i(r), \quad 2\varepsilon_{zr}(r,z,t) \\ &= \frac{\partial U_i(z,t)}{\partial z}\varphi_i(r) + W_i(z,t)\frac{d\varphi_i(r)}{dr} \end{aligned} \tag{4}$$

where $\varepsilon_i (i = r, \theta, z)$ and ε_{zr} are the strain vector components. The stress vector is related to the strain vector by using the constitutive relations in the case of axial symmetry:

$$\begin{Bmatrix} \sigma_r \\ \sigma_\theta \\ \sigma_z \\ \sigma_{zr} \end{Bmatrix} = \begin{bmatrix} C_{11} & C_{12} & C_{13} & 0 \\ & C_{22} & C_{23} & 0 \\ & & C_{33} & 0 \\ Sym. & & & C_{55} \end{bmatrix} \begin{Bmatrix} \varepsilon_r \\ \varepsilon_\theta \\ \varepsilon_z \\ 2\varepsilon_{zr} \end{Bmatrix} \tag{5}$$

where $\sigma_i (i = r, \theta, z)$ and σ_{zr} are the stress vector components and the elastic coefficients are defined as:

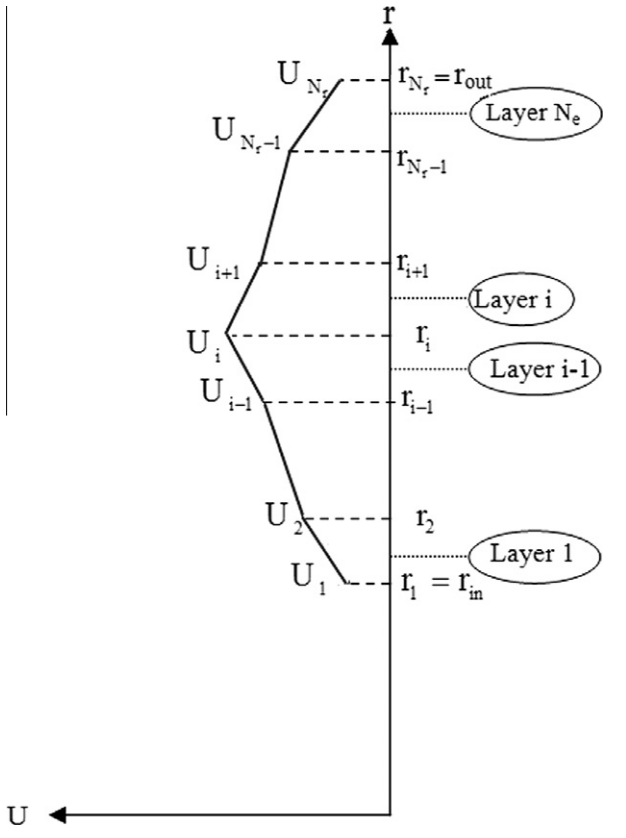

Fig. 2. The through-thickness approximation of the displacement field.

$$C_{mm} = \frac{(1-\nu)E(r)}{(1+\nu)(1-2\nu)}, \quad C_{mn} = \frac{\nu C_{mm}}{(1-\nu)},$$
$$C_{55} = \frac{E(r)}{2(1+\nu)} \quad (m,n = 1,2,3) \tag{6}$$

The equations of motions together with the related boundary conditions are determined by using Hamilton's principle:

$$\int_{t_o}^{t_1} (\delta T - \delta(V+L))\, dt = 0 \tag{7}$$

where T is the kinetic energy, V denotes the elastic strain energy, L stands for the potential energy of external forces and δ is the variational symbol. Also t_0 and t_1 are two arbitrary times. The kinetic energy, the elastic strain energy and the potential energy of the external forces are defined by the following relations:

$$\delta T = 2\pi \int_0^l I^{ij}(\dot{U}_i \delta \dot{U}_j + \dot{W}_i \delta \dot{W}_j)\, dz \tag{8}$$

$$\delta V = 2\pi \int_0^l \int_{r_{in}}^{r_{out}} (\sigma_r \delta\varepsilon_r + \sigma_\theta \delta\varepsilon_\theta + \sigma_z \delta\varepsilon_z + 2\sigma_{rz}\delta\varepsilon_{rz})\, r\, dr dz \tag{9}$$

$$\delta L = -2\pi \cdot \left(r_{in} P_{in}(t)\delta_{j1} + r_{out} P_{ext}(t)\delta_{jN_r}\right) \int_0^l \delta U_j\, dz \tag{10}$$

where $I^{ij} = \int_{r_{in}}^{r_{out}} \rho \varphi_i \varphi_j r\, dr$, $P_{in}(t)$ and $P_{ext}(t)$ are internal and external dynamic pressures, and δ_{ij} is the Kronecker delta. In this paper dot over a variable denotes the partial differentiation with respect to time (t). By substituting Eqs. (8)–(10) into Eq. (7) and carrying out a typical variation process, the governing equations of motion together with the related boundary conditions are derived. Also in the Hamilton's principle, initial conditions are assumed to be known.

- Governing equations:

$$-C_{11}^{ij}U_i - E_{22}^{ij}U_i - F_{12}^{ij}U_i - F_{21}^{ji}U_i - B_{31}^{ji}\frac{\partial W_i}{\partial z} - D_{32}^{ij}\frac{\partial W_i}{\partial z} + A_{55}^{ij}\frac{\partial^2 U_i}{\partial z^2} + B_{55}^{ij}\frac{\partial W_i}{\partial z} + r_{in}P_{in}(t)\delta_{j1} - r_{out}P_{ext}(t)\delta_{jNr} = I^{ij}\ddot{U}_i \tag{11}$$

$$B_{13}^{ij}\frac{\partial U_i}{\partial z} + D_{23}^{ij}\frac{\partial U_i}{\partial z} + A_{33}^{ij}\frac{\partial^2 W_i}{\partial z^2} - B_{55}^{ji}\frac{\partial U_i}{\partial z} - C_{55}^{ij}W_i = I^{ij}\ddot{W}_i \tag{12}$$

- Boundary conditions at the ends $z = 0$ and l:

$$\text{Either } U_j = 0 \quad \text{or} \quad A_{55}^{ij}\frac{\partial U_i}{\partial z} + B_{55}^{ij}W_i = 0 \tag{13}$$

$$\text{Either } W_j = 0 \quad \text{or} \quad B_{13}^{ij}U_i + D_{23}^{ij}U_i + A_{33}^{ij}\frac{\partial W_i}{\partial z} = 0 \tag{14}$$

where

$$A_{mn}^{ij} = \int_{r_{in}}^{r_{out}} C_{mn}\varphi_i\varphi_j r\, dr, \quad B_{mn}^{ij} = \int_{r_{in}}^{r_{out}} C_{mn}\frac{\partial\varphi_i}{\partial r}\varphi_j r\, dr,$$
$$C_{mn}^{ij} = \int_{r_{in}}^{r_{out}} C_{mn}\frac{\partial\varphi_i}{\partial r}\frac{\partial\varphi_j}{\partial r} r\, dr, \quad D_{mn}^{ij} = \int_{r_{in}}^{r_{out}} C_{mn}\varphi_i\varphi_j\, dr,$$
$$E_{mn}^{ij} = \int_{r_{in}}^{r_{out}} C_{mn}\frac{\varphi_i\varphi_j}{r}\, dr, \quad F_{mn}^{ij} = \int_{r_{in}}^{r_{out}} C_{mn}\frac{\partial\varphi_i}{\partial r}\varphi_j\, dr \tag{15}$$

2.3. The DQM discretized form of the equations of motion

At this stage, the governing differential equations and the related boundary conditions are discretized into algebraic equations using DQM. In this method, the first and second-order partial derivatives of a field variable at the ith discrete point in the computational domain are approximated by a weighted linear summation of the field variable at all discrete nodes located along the line that passes through that point in the domain. Using the DQ discretization rules for spatial derivatives [16–18], the equations of motion for an arbitrary layer i, at each domain grid point z_m and time moment t_p are obtained ($m = 1, 2, \ldots, N_z$, $n = 1, 2, \ldots, N_z$, $p = 1, 2, \ldots, N_t$).

$$\frac{\partial U_{imp}(z_m,t_p)}{\partial z} = a_{mn}U_{inp}, \quad \frac{\partial^2 U_{imp}(z_m,t_p)}{\partial z^2} = b_{mn}U_{inp}$$
$$\frac{\partial W_{imp}(z_m,t_p)}{\partial z} = a_{mn}W_{inp}, \quad \frac{\partial^2 W_{imp}(z_m,t_p)}{\partial z^2} = b_{mn}W_{inp} \tag{16}$$

where N_z is the number of grid points in the axial direction. Generally, the dynamical systems of equations are solved using the finite difference based time integration schemes. Recently, Malekzadeh et al. [18] employed DQM as a simple and efficient way to impose the initial condition without changing the formulation of the conventional DQM. Based on this approach, the whole time domain is divided into a set of temporal sub-domain N_D. Afterwards, each time sub-domain is discretized into N_t grid points. At any grid point, the time derivatives are discretized according to the conventional DQ rules. Thus, the second-order derivative of a field variable $\xi_{im}(t)$ is discretized as follows:

$$\begin{aligned}\ddot{\xi}_{imp}(z_m,t_p) &= \sum_{q'=1}^{N_t} A_{pq'}^t \dot{\xi}_{imq'}(z_m,t_{q'}) \\ &= A_{p1}^t \dot{\xi}_{im1}(z_m,t_1) + \sum_{q'=2}^{N_t} A_{pq'}^t \dot{\xi}_{imq'}(z_m,t_{q'}) \\ &= A_{p1}^t \dot{\xi}_{im1} + B_{p1}^t \xi_{im1} + B_{pq}^t \xi_{imq}\end{aligned} \tag{17}$$

where $q = 2, 3, \ldots, N_t$, $B_{pk}^t = \sum_{s=2}^{N_t} A_{ps}^t A_{sq}^t$ and A_{pq}^t are the weighting coefficient of the first-order derivative. Also ξ_{im1} and $\dot{\xi}_{im1}$ are the initial values of the field variable. Following the above procedure, the

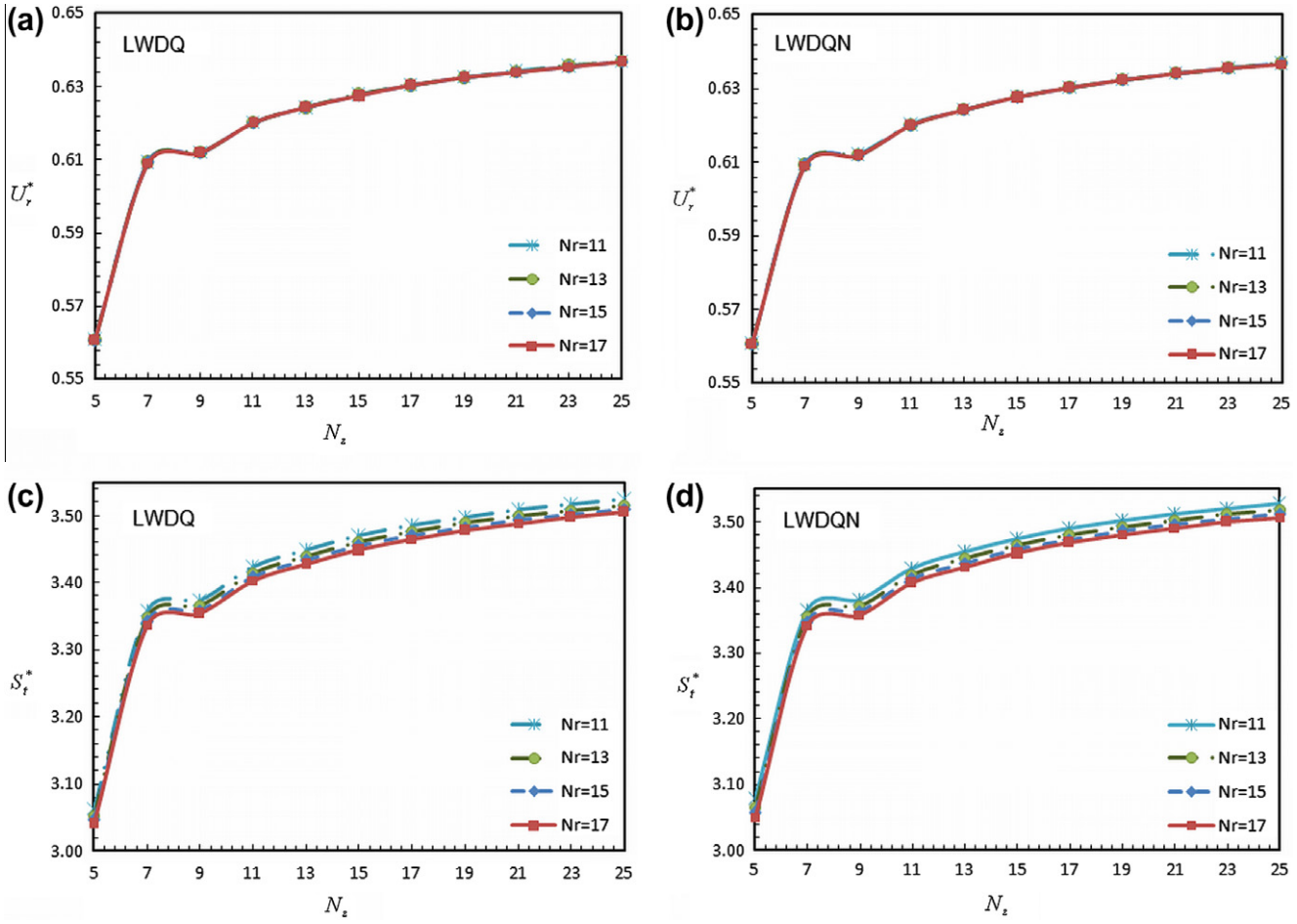

Fig. 3. (a–d) The convergence behavior of non-dimensional maximum radial displacement and tangential stress for LWDQ and LWDQN codes.

final DQ form of the governing equations and boundary conditions are developed.

- Governing equations:

$$\left(C_{11}^{ij}U_{inq}+E_{22}^{ij}U_{inq}+F_{12}^{ij}U_{inq}+F_{21}^{ji}U_{inq}\right)\delta_{mn}\delta_{pq}+\left(B_{31}^{ji}a_{mn}W_{inq}+D_{32}^{ij}a_{mn}W_{inq}A_{55}^{ij}b_{mn}U_{inq}-B_{55}^{ij}a_{mn}W_{inq}\right)\delta_{pq}+I^{ij}\left(A_{p1}^{t}\dot{U}_{in1}+B_{p1}^{t}U_{in1}+B_{pq}^{t}U_{inq}\right)\delta_{mn}=r_{in}P_{in}(t)\delta_{j1}-r_{out}P_{ext}(t)\delta_{jNr} \quad (18)$$

$$\left(-B_{13}^{ij}a_{mn}U_{inq}-D_{23}^{ij}a_{mn}U_{inq}-A_{33}^{ij}b_{mn}W_{inq}+B_{55}^{ji}a_{mn}U_{inq}+C_{55}^{ij}W_{inq}\delta_{mn}\right)\delta_{pq}+I^{ij}\left(A_{p1}^{t}\dot{W}_{in1}+B_{p1}^{t}W_{in1}+B_{pq}^{t}W_{inq}\right)\delta_{mn}=0 \quad (19)$$

- Boundary conditions at the ends $z = 0$ and l:

$$\text{Either } U_{imp}=0 \quad \text{or} \quad A_{55}^{ij}a_{mn}U_{inq}+B_{55}^{ij}W_{imp}=0 \quad (20)$$

$$\text{Either } W_{imp}=0 \quad \text{or} \quad B_{13}^{ij}U_{imp}+D_{23}^{ij}U_{imp}+A_{33}^{ij}a_{mn}W_{inq}=0 \quad (21)$$

Table 1
Radial displacement vs. thickness of the shell.

r (m)	U_r (mm)			
	LWDQ	LWDQN	Exact [12]	ANSYS
0.250	0.136	0.138	0.136	0.136
0.300	0.118	0.119	0.118	0.118
0.350	0.105	0.106	0.105	0.106
0.400	0.097	0.097	0.097	0.097
0.450	0.091	0.091	0.091	0.091
0.500	0.086	0.086	0.086	0.087

By substituting the boundary conditions to the DQ form of governing equations, a system of algebraic equations with $2N_DN_r(N_z-2)(N_t-1)$ equations and unknowns is derived. Then, the time histories of the radial and axial displacements at each grid point are determined by solving the system of equations. Eventually, the strain and stress components at each point of the cylindrical shell are predicted using Eqs. (2)–(5). In this paper, three common types of boundary conditions at the ends of the FG shell ($z = 0, l$) are investigated:

(a) Clamped boundary condition (C–C): this type of boundary condition is as follows:

$$U_{imp}=W_{imp}=0 \quad \text{at} \quad z=0,l \quad (22)$$

(b) Simply supported boundary condition (S–S(1)): In this case, boundary conditions for the mid radial grids are the same as the clamped boundary condition and for the other radial grids located in boundaries are as follows:

$$A_{55}^{ij}a_{mn}U_{inq}+B_{55}^{ij}W_{imp}=W_{imp}=0 \quad \text{at} \quad z=0,l \quad (23)$$

Table 2
Geometric parameters and material properties of the FG shell.

E_m (GPa)	E_c (GPa)	ρ_m (kg/m^3)	ρ_c (kg/m^3)	ν_m	ν_c	n_1	n_2	l (m)	r_{in} (m)	r_{out} (m)
223	348.44	8900	2369.81	0.3	0.3	2	−5.93	1	0.08	0.1

Table 3
Dimensionless maximum radial displacement and stress components at the inner surface of the cylinder mid-length.

t^*	U_r^*			S_r^*			S_t^*			S_z^*		
	LWDQ	LWDQN	ANSYS	LWDQ	LWDQN	ANSYS	LWDQ	LWDQN	ANSYS	LWDQ	LWDQN	ANSYS
0.1	0.196	0.196	0.201	−0.290	−0.287	−0.296	1.082	1.082	1.109	0.237	0.242	0.232
0.2	0.373	0.373	0.384	−0.554	−0.546	−0.562	2.058	2.059	2.109	0.452	0.461	0.440
0.3	0.505	0.505	0.525	−0.748	−0.739	−0.774	2.783	2.784	2.903	0.611	0.623	0.606
0.4	0.589	0.589	0.610	−0.874	−0.862	−0.909	3.248	3.250	3.413	0.713	0.727	0.708
0.5	0.637	0.637	0.652	−0.945	−0.932	−0.956	3.510	3.512	3.589	0.771	0.786	0.749

(c) Simply supported boundary condition (S–S(2)): In this case, boundary conditions for the mid radial grids are the same as clamped boundary condition and for the other radial grids located in boundaries are as follows:

$$U_{imp} = B_{13}^{ij} U_{imp} + D_{23}^{ij} U_{imp} + A_{33}^{ij} a_{mn} W_{inq} = 0 \quad \text{at} \quad z = 0, l \tag{24}$$

2.4. Newmark's time integration method

As an alternative method and in order to obtain a comparative solution, Newmark's time integration scheme is applied in the time domain to the DQ discretized form of the governing equations and the related boundaries.

$$\begin{aligned}&\left(C_{11}^{ij} U_{inp} + E_{22}^{ij} U_{inp} + F_{12}^{ij} U_{inp} + F_{21}^{ji} U_{inp}\right)\delta_{mn} + B_{31}^{ji} a_{mn} W_{inp} \\ &+ D_{32}^{ij} a_{mn} W_{inp} - A_{55}^{ij} b_{mn} U_{inp} - B_{55}^{ij} a_{mn} W_{inp} - r_{in} P_{in}(t)\delta_{j1} \\ &+ r_{out} P_{ext}(t)\delta_{jNr} = -I^{ij} \ddot{U}_{imp}\end{aligned} \tag{25}$$

$$\begin{aligned}&B_{55}^{ji} a_{mn} U_{inp} - B_{13}^{ij} a_{mn} U_{inp} - D_{23}^{ij} a_{mn} U_{inp} - A_{33}^{ij} b_{mn} W_{inp} + C_{55}^{ij} W_{inp}\delta_{mn} \\ &= -I^{ij} \ddot{W}_{imp}\end{aligned} \tag{26}$$

In this procedure, the dynamical system of Eqs. (25) and (26) at time $(t + t_0)$ is solved according to the Eqs. (27) and (28).

$$\begin{aligned}\{\ddot{U}_{t+t_1}\} &= a_0(\{U_{t+t_1}\} - \{U_t\}) - a_2\{\dot{U}_t\} - a_3\{\ddot{U}_t\}, \\ \{\dot{U}_{t+t_1}\} &= \{\dot{U}_t\} + a_6\{\ddot{U}_t\} + a_7\{\ddot{U}_{t+t_1}\}\end{aligned} \tag{27}$$

$$\begin{aligned}&a_0 = \frac{1}{\alpha \Delta t^2}, \quad a_1 = \frac{\delta}{\alpha \Delta t}, \quad a_2 = \frac{1}{\alpha \Delta t}, \quad a_3 = \frac{1}{2\alpha} - 1 \\ &a_4 = \frac{\delta}{\alpha} - 1, \quad a_5 = \frac{\Delta t}{2}\left(\frac{\delta}{\alpha} - 2\right), \quad a_6 = \Delta t(1 - \delta), \quad a_7 = \delta \Delta t\end{aligned} \tag{28}$$

In Eq. (28), Δt is time step, α and δ are time integration parameters which are set equal to, $\alpha = 0.25(1 + \gamma)^2$ and $\delta = 0.5 + \gamma$ with $\gamma = 0.005$.

3. Numerical results

In this section, numerical results are presented for the transient dynamic response of FG circular cylindrical shells under internal or external dynamic pressure. Two solution methods are used: (1) DQM for both spatial coordinates and time domain (LWDQ) and

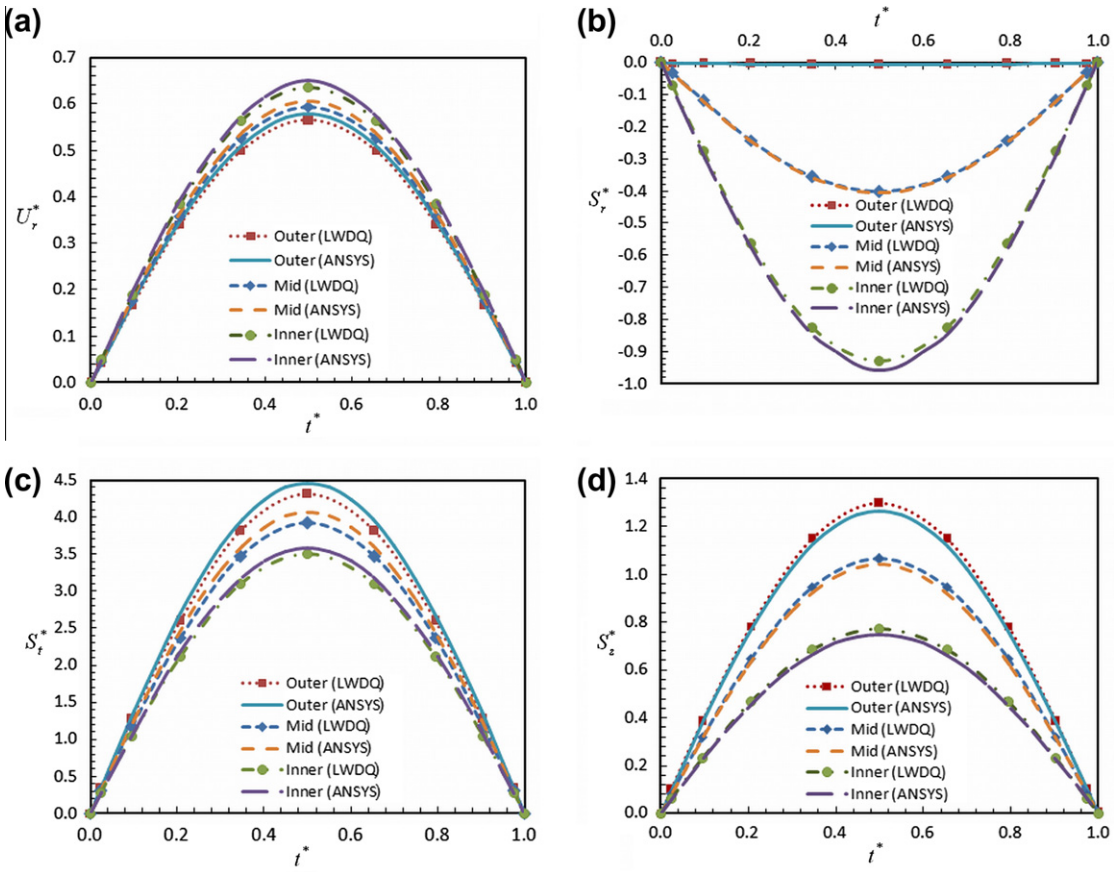

Fig. 4. Time histories of non-dimensional (a) radial displacement, (b) radial stress, (c) tangential stress and (d) axial stress at the inner, mid and outer surfaces of the cylinder mid-length obtained by LWDQ and ANSYS.

Table 4
Through thickness variation of dimensionless radial displacement and stress components at the mid-length of cylinder using LWDQ.

r^*	U_r^*	S_r^*	S_t^*	S_z^*
1.00	0.637	−0.944	3.510	0.782
1.05	0.618	−0.752	3.674	0.895
1.10	0.602	−0.560	3.841	1.006
1.15	0.588	−0.367	4.011	1.115
1.20	0.576	−0.170	4.185	1.223
1.25	0.566	−0.040	4.309	1.291

(2) spatial DQ discretized form of the equations and Newmark's time integration scheme in the time domain (LWDQN).

As a first step, the correctness and accuracy of the present method are demonstrated. Due to lack of solutions similar to the present work, comparisons with exact solution of an isotropic cylindrical shell with infinite length are carried out. Then, the convergence study and further analyses are performed.

3.1. Validation

To validate the present model, comparisons with the exact solution of Shahabian and Hosseini et al. [12] and the results of ANSYS for an isotropic cylindrical shell with infinite length are carried out. The cylinder is made of Aluminum with $E = 70$ GPa, $\rho = 2700$ kg/m^3, and has an inner and outer radii of 0.25 m and 0.5 m, respectively. It is internal dynamic pressure of $P(t) = 20(1 - e^{-10^5 t})$ (MPa).

In Table 1, the radial displacements at different points of the shell thickness are obtained and compared with the exact solution in Ref. [12] and ANSYS results. To obtain the finite element results, 3D solid elements with 20 nodes are used. The presented solutions show a very good agreement with the both reference exact solution and ANSYS results. The LWDQ method yields more accurate results which agree with the exact solution to three significant digits accuracy.

The convergence behavior of the predicted maximum radial displacement and tangential stress are examined in Fig. 3 for both the LWDQ and LWDQN methods. The grid points in the axial direction are varied from 5 to 25 while the number of nodes across the thickness is considered to be $N_r = 11$, 13, 15 and 19. It is seen that the radial displacement is converges already with 11 grid points through the thickness of the cylinder. According to the results, the grid points density of $N_r = 11$, $N_z = 25$ is suitable for the displacement components while $N_r = 15$, $N_z = 25$ is appropriate in the case of the stress components. The convergence behavior is similar for both methods. The accuracy of LWDQ is higher than LWDQN.

By changing dimensionless time steps from 0.05 to 0.04 in both LWDQ and LWDQN codes, no variation in the displacement and stress components are observed. A dimensionless time step equal to 0.05 is, therefore, selected. For the sake of brevity, these results are not shown here.

3.2. FG shell

In the second example, FG shells are modeled using the commercial finite element software of ANSYS. One-quadrant of the shell structure is simulated using 18,000 3D solid elements with 20 nodes. Also, the thickness of the cylinder is divided into 15 layers, and the properties of each layer are assumed to be identical to the properties of the layer middle-plane.

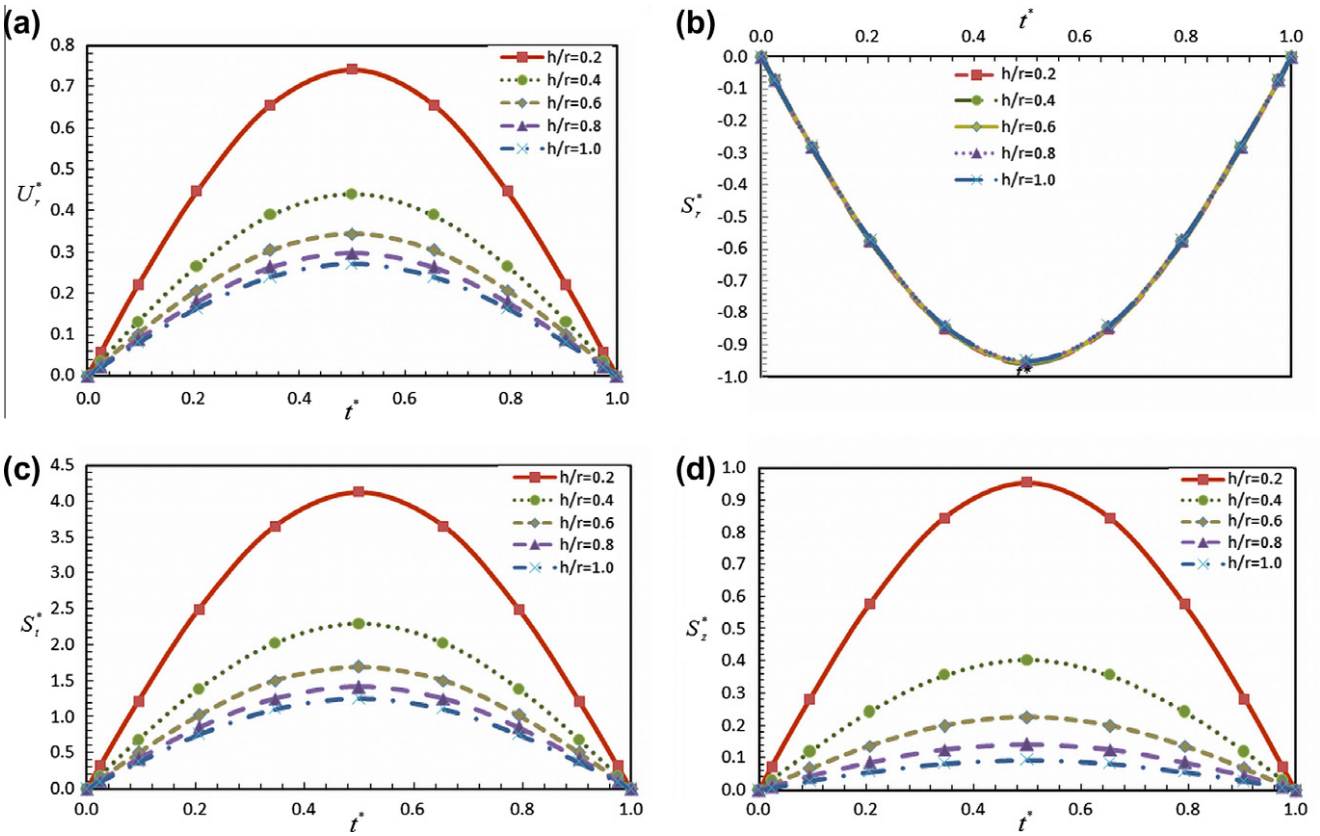

Fig. 5. Time histories of the non-dimensional (a) radial displacement, (b) radial stress, (c) tangential stress and (d) axial stress at the inner surface of the cylinder mid-length with different h/r_{in} ratios ($r_{in} = 0.08$ m and $l = 1$ m).

In this part, the shell is assumed to be composed of silicon nitride (Si_3N_4) on outer surface and nickel on inner surface. Furthermore, the initial displacements and velocities are assumed to be zero. The geometric parameters and material properties of the FG shell are shown in Table 2. The cylinder is subjected to a sinusoidal transient dynamic internal pressure $P(t)$ for a time duration of 1 s as:

$$P(t) = P_0 \sin(\pi t) \tag{29}$$

In the analysis, cylinders with clamped boundary conditions are considered, unless otherwise stated. The following non-dimensional parameters are used:

$$t^* = \frac{t}{t_e}, \quad z^* = \frac{z}{L}, \quad r^* = \frac{r}{r_{in}}, \quad U_i^* = \frac{u_i}{P_o h/k^*} \quad (i = r, z), \quad S_i^* = \frac{\sigma_i}{P_0} \quad (i = r, \theta, z) \tag{30}$$

where t_e is loading time duration and $k^* = 10$ GPa.

In Table 3, the time history of the non-dimensional radial displacement and radial, axial and tangential stress components at the inner surface of the cylinder mid-length is presented. The results of the two developed codes are compared with those obtained by ANSYS. All solutions exhibit close agreements. The maximum difference between the LWDQ predictions and those of FEM is about 4.8% for the case of the tangential stress. In the FEM modeling, the properties of each layer are considered to be equal to the properties of its mid surface. A step-wise approximation of the material gradation represents a further approximation in the FE model. This type of solution requires a high computational cost. The total CPU time for dynamic analysis of considered FG shell is 40 s using the LWDQ method. On the other hand, finite element software of ANSYS uses 28 times more CPU time than the LWDQ code for the same problem.

Fig. 4 depicts time histories of the non-dimensional radial displacement and stress components at the inner, mid and outer surfaces of the cylinder mid-length. The results predicted by the LWDQ algorithm are compared with those obtained by the ANSYS software. It is observed that the dominant component of stress is the circumferential one.

In Table 4, through-the-thickness variations of the non-dimensional radial displacement and stress components at the mid-length of cylinder are presented using LWDQ code. It is seen that the largest values of the axial and circumferential stresses occur at the outer surface due to the higher stiffness of ceramic compared to the inner metal rich face.

The time response of the FG cylinder with different ratios of thickness to inner radius is illustrated in Fig. 5. The non-dimensional radial displacement and stress components at the inner surface of the cylinder mid-length with inner radius of 0.08 m and length of 1 m are determined. Both moderately thick and thick shells are considered. As expected, the radial displacement and stress components decrease with increasing thickness but the variation of the radial stress is not significantly changed. Fig. 5 shows that h/r_{in} ratio has considerable effect on the magnitudes of the displacement and stress components. This effect increases for the smaller values of the h/r_{in} ratios.

To investigate the influence of some commonly used boundary conditions, the transient dynamic response of the FG cylinder for clamped and two types of simply supported boundary conditions are predicted. Time histories of the non-dimensional radial displacement and tangential stress at the inner surface of the cylinder mid-length for the three described boundary conditions are shown in Fig. 6. Furthermore, Fig. 7 illustrates the non-dimensional radial and axial displacements as well as the dimensionless tangential and radial stresses at the inner surface of the cylinder length with different types of boundary conditions at $t^* = 0.5$.

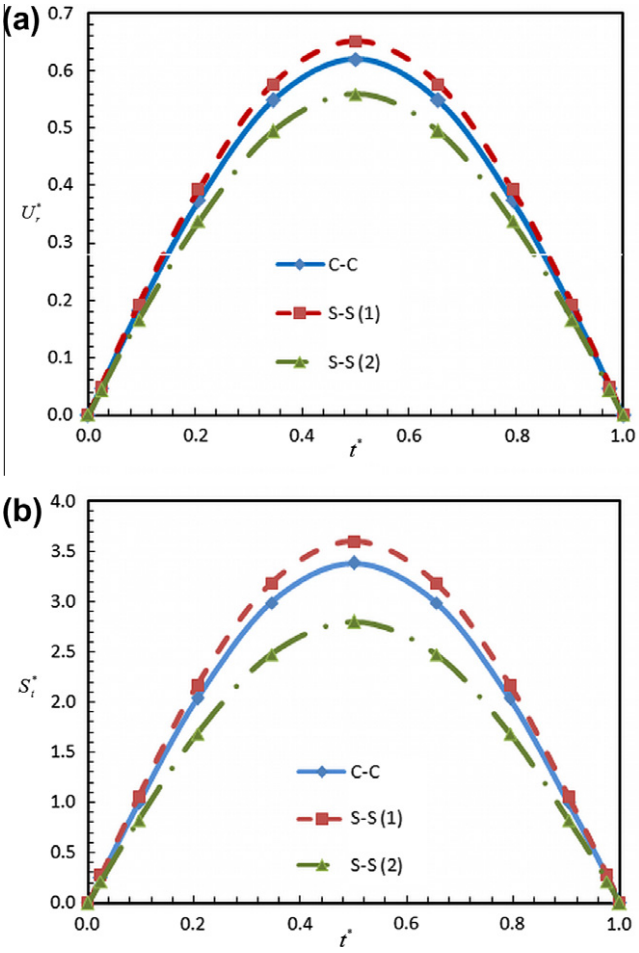

Fig. 6. Time histories of the non-dimensional (a) radial displacement and (b) tangential stress at the inner surface of the cylinder mid-length for the three described boundary conditions.

It is observed that the distribution of the radial stress far from the ends exhibits a very low dependency on the type of boundary condition. It is also seen that both the clamped and the simply support type-1 predict close distributions for the non-dimensional radial and tangential stresses.

4. Conclusions

A layerwise-differential quadrature method is developed for transient dynamic response of functionally graded cylindrical shells subjected to dynamic pressure. Both DQM and Newmark's integration scheme are separately employed to discretize the DQ governing equations of motion in the time domain. It is found that both the approaches present a fast rate of convergence and yield accurate results when compared with the solutions of ANSYS software. In comparison with the finite element simulations that need very fine meshes, considerable less computation cost of the present solutions exhibits efficiency of the methodology. Also, layerwise theory provides the capability of precise modeling of moderately thick and thick FG shells. It is observed that the two approaches yield very close results, although the LWDQ method yields more accurate results than the LWDQN one does. The effects of geometrical parameters and boundary conditions have been also investigated. It is seen that the distribution of the radial stress far from

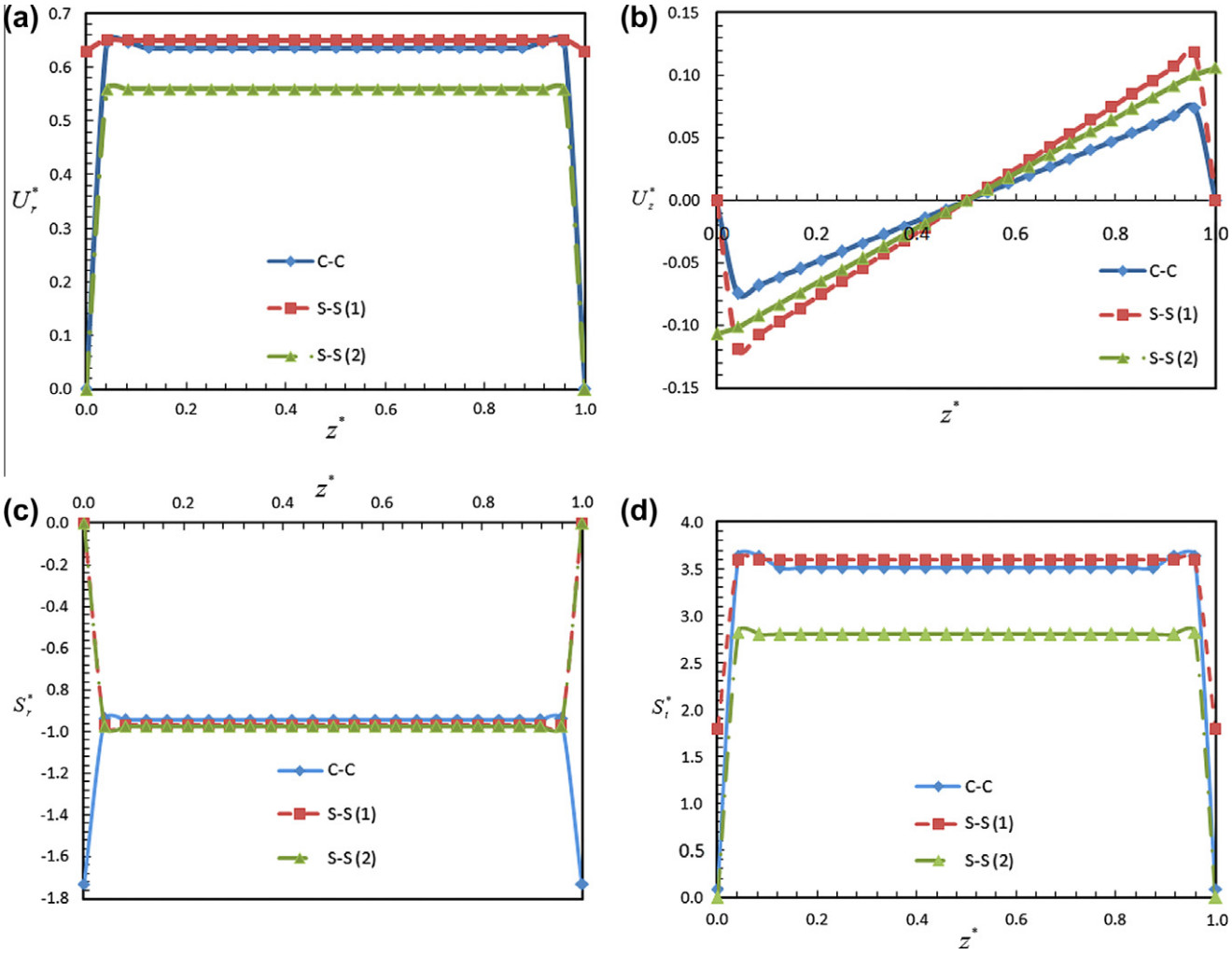

Fig. 7. Distributions of the non-dimensional (a) radial displacement, (b) radial stress, (c) tangential stress and (d) axial stress at the inner surface of the cylinder length for three types of boundary conditions at $t^* = 0.5$.

the ends shows a very low dependency on the boundary condition type. The presented results can be used as benchmark solutions for future works.

References

[1] Reddy JN. Mechanics of laminated composite plates and shells: theory and analysis. CRC Press; 1997.

[2] Qatu MS, Sullivan RW, Wang W. Recent research advances on the dynamic analysis of composite shells: 2000–2009. Compos Struct 2010;93:14–31.

[3] Awaji H, Sivakuman R. Temperature and stress distributions in a hollow cylinder of functionally graded material: the case of temperature-dependent material properties. J Am Ceram Soc 2001;84:1059–65.

[4] Sofiyev AH, Schnack E. The stability of functionally graded cylindrical shells under linearly increasing dynamic torsional loading. Eng Struct 2004;26:1321–31.

[5] Wang BL, Mai YW, Zhang XH. Thermal shock resistance of functionally graded materials. Acta Mater 2004;52:4961–72.

[6] Zhu JQ, Chen C, Shen YP, Wang SL. Dynamic stability of functionally graded piezoelectric circular cylindrical shells. Mater Lett 2005;59:477–85.

[7] Bahtui A, Eslami MR. Coupled thermoelasticity of functionally graded cylindrical shells. Mech Res Commun 2007;34:1–18.

[8] Santos H, Mota Soares CM, Mota Soares CA, Reddy JN. A semi-analytical finite element model for the analysis of cylindrical shells made of functionally graded materials under thermal shock. Compos Struct 2008;86:10–21.

[9] Guo LC, Noda N. An analytical method for thermal stresses of a functionally graded material cylindrical shell under a thermal shock. Acta Mech 2010;214:71–8.

[10] Peng XL, Li XF. Transient response of temperature and thermal stresses in a functionally graded hollow cylinder. J Therm Stress 2010;33:485–500.

[11] Hosseini SM, Shahabian F. Reliability of stress field in Al–Al_2O_3 functionally graded thick hollow cylinder subjected to sudden unloading, considering uncertain mechanical properties. Mater Des 2010;31:3748–60.

[12] Shahabian F, Hosseini SM. Stochastic dynamic analysis of a functionally graded thick hollow cylinder with uncertain material properties subjected to shock loading. Mater Des 2010;31:894–901.

[13] Basar Y, Omurtag MH. Free-vibration analysis of thin/thick laminated structures by layer-wise shell models. Comput Struct 2000;74:409–27.

[14] Tahani M, Mirzababaee SM. Non-linear analysis of functionally graded plates in cylindrical bending under thermomechanical loadings based on a layerwise theory. Eur J Mech A/Solids 2009;28:248–56.

[15] Bert CW, Malik M. Differential quadrature method in computational mechanics: a review. Appl Mech Rev 1996;49:1–27.

[16] Bert CW, Malik M. Differential quadrature method: a powerful new technique for analysis of composite structures. Compos Struct 1997;39:179–89.

[17] Malekzadeh P, Farid M, Zahedinejad P. A three-dimensional layerwise-differential quadrature free vibration analysis of laminated cylindrical shells. Int J Press Vessels Pip 2008;85:450–8.

[18] Malekzadeh P, Fiouz AR, Razi H. Three-dimensional dynamic analysis of laminated composite plates subjected to moving load. Compos Struct 2009;90:105–14.

[19] Malekzadeh P. Three-dimensional free vibration analysis of thick functionally graded plates on elastic foundations. Compos Struct 2009;89:367–73.

[20] Malekzadeh P, Alibeygi Beni A. Free vibration of functionally graded arbitrary straight-sided quadrilateral plates in thermal environment. Compos Struct 2010;92:2758–67.

[21] Malekzadeh P, Shahpari SA, Ziaee HR. Three-dimensional free vibration of thick functionally graded annular plates in thermal environment. J Sound Vib 2010;329:425–42.